JOURNAL OF COMPUTATIONAL PHYSICS 4, 147–170 (1969)

Two Dimensional Wave Propagation through Nonlinear Media

CARL J. COSTANTINO

Civil Engineering Department, City College of New York, New York, New York 10031

Received October 15, 1968

INTRODUCTION

This report describes the development of a large computer program to treat the two dimensional stress wave propagation problem in arbitrary nonlinear media. The computer code, termed the SLAM Code for identification, is based upon the finite element approach to the stress wave problem and can treat either the axisymmetric or plane (stress or strain) configuration.

The finite element approach has been taken in this development to allow the user a general flexibility in treating two dimensional problems of rather complex geometry (inclusions, material layering, complex boundaries, etc.). The primary objective of this study has been to develop a code to treat ground shock effects caused by a high energy explosion, although it is quite obvious that the program has applicability to other stress wave problems. Nonetheless, for the primary problems of interest, the half-space to which the loadings are applied generally consists of several (arbitrarily oriented) layers of soil/rock materials, each with significantly differing nonlinear properties.

The majority of codes that have been developed to treat these problems are based upon finite difference formulations, and thus would have difficulty in treating these complex geometries. In addition, an added flexibility has been built into the SLAM code, and this concerns the specification of material properties. A catalogue of material constitutive laws has been developed which can be added to with little difficulty withough changing the operation of the code. Each material occurring in a particular problem can then be allowed to have any of the material properties available in the catalogue.

Of course, this brings up a major problem when dealing with earth materials, namely, the specification of applicable constitutive relations. The current catalogue allows the specification of the following constitutive relations:

(a) isotropic elastic material,

581/4/2-1

(b) transverse isotropic elastic material,

(c) linear compressible fluid,

(d) linear viscoelastic material,

(e) elastic plastic material satisfying the Mises yield criterion with arbitrary strain hardening.

(f) elastic plastic material satisfying the Coulomb-Mohr yield criterion.

(g) a nonlinear material law which contains a stiffening effect under hydrostatic pressure as well as a plastic dissipation under deviatoric strains, to account for compaction effects in soils.

The last three of this list are the only nonlinear laws currently available in the code, and it is with materials (e) and (f) that this report will be concerned. However, all of these constitutive relations have been included in an attempt to at least crudely approximate some known responses of soil-rock materials. Quite apparently, none of these are completely adequate but until further advances in the state of the art occur, only such approximations are available for applications to earth media.

The use of the catalogue formulation is extremely advantageous and allows easy expansion of the capability of the code as further developments in constitutive relationships occur. The acronyn SLAM was therefore chosen to try to indicate the applicability of the code, representing the phrase *S*tress Waves in *L*ayered *A*rbitrary *M*edia.

The initial formulation of the SLAM Code was based upon the elastic two dimensional problem [*1*]. This was done to develop the general flow and operation of the computer program. After this development, the inclusion of material nonlinearities was made.

In order to arrive at a mesh with which to attack a given problem, the two dimensional configuration is divided into small elements, these elements being connected at their vertices to each other. In the SLAM Code, rectangular and triangular elements are used for the mesh formulation. The data that is then developed is the motion history (displacements, velocities, accelerations, stresses, etc.) at these node points or vertices. This method of mesh formation is essentially a physical one, as opposed to the more abstract approach of finite difference methods. Of course, if a uniform element mesh is chosen (uniform spacing of nodes), the developed equations of motion are entirely analogous to a finite difference formulation.

The code has been designed to treat up to 1000 nodes (2000 degrees of freedom) with no restriction being placed on the number of elements comprising the mesh. This upper bound on the number of nodes was chosen in an arbitrary fashion, being more than enough to treat the problems investigated to date. This figure can be rather easily extended to allow many more nodes in the mesh but no requirement

for such extension has been encountered as yet. The code has been made operational on the IBM 7094, CDC 3600 and CDC 6600 computers.

In comparing the finite element formulation with its counterpart finite difference formulation, one important consideration must be kept in mind. The primary advantage of the finite element approach lies in its flexibility in specifying node distributions for a particular problem. Thus it can be used to treat problems of as complex a geometry as desired with no change in computer code formulation. However, this added flexibility is obtained at a cost, this cost being the increased amount of information that must be maintained in the computer (or its auxiliary storage units). Thus, to perform a calculation for a simple problem with, say, a uniform mesh, the finite element formulation will be inefficient as compared to finite differences. For problems where simple mesh formations can be used, the finite element solution will in general take more machine time to achieve the same results as the difference solution. Thus the very flexibility which is its advantage can be considered a disadvantage for these cases.

Material Nonlinearity Effects

As mentioned previously, the SLAM Code was originally developed for application to elastic materials [*1*]. The extension of the analysis to include material nonlinearities is presented herein. The notation used follows from the previously reported results [*1*]. In the analysis, any material constitutive law can be used, provided of course that it can be suitably described for inclusion in the code. Two particular laws are presented herein, both being elastic-plastic relations. The first is characterized by the Prandtl–Reuss relations [*2*] (von Mises yield criterion) and the second by the Coulomb–Mohr yield criterion [*3*] and its associated flow rule.

The computational procedure starts from some time at which the complete solution is known; that is, the displacements, velocities and accelerations of all the nodes are specified, as well as the entire stress and strain history up to and including this time. Typically this time is the zero or initial time, although it need not be. The problem then is to determine these same variables at the following instant of time, suitably taking into account the nonlinearities introduced by the material properties.

In the following presentation, the analysis will be carried forth considering a typical triangular element of the freefield mesh, for convenience. The development for the general rectangular element used in the analysis (or for that matter any other element shape desired) follows in a straight forward manner. The reader is referred to the previous development [*1*].

The displacement field assumed for the triangular element (Fig. 1) is a linear one which can be written as

$$\begin{Bmatrix} u \\ w \end{Bmatrix} = \begin{bmatrix} \alpha_1 & \alpha_2 & \alpha_3 \\ \alpha_4 & \alpha_5 & \alpha_6 \end{bmatrix} \begin{Bmatrix} 1 \\ r \\ z \end{Bmatrix} \tag{1}$$

where u is the horizontal displacement of any interior point of the element specified by the local coordinates (r, z), w is the corresponding vertical displacement and α_i are six arbitrary constants. Positive displacements are taken in the positive

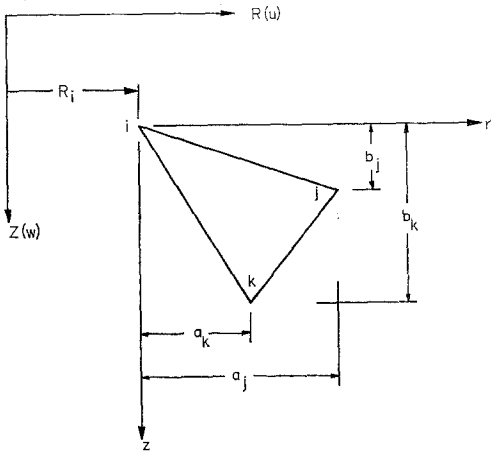

FIG. 1. General triangular element.

(R, Z) directions, which are the system or global coordinates (Fig. 1). Substituting the node point coordinates in Eq. (1), the unknown coefficients, α_i, can be determined in terms of the node point displacements as

$$\{\alpha\} = [D]\{x\} \tag{2}$$

where

$$\{\alpha\} = \{\alpha_1, \alpha_2, \ldots, \alpha_6\}$$

$$\{x\} = \{u_i, w_i, u_j, w_j, u_k, w_k\}$$

and D is a 6×6 matrix defined by the element geometry [1].

The strains developed at any point within the element can be determined from

the specified displacement field of Eq. (1). For the axisymmetric problem, for example, these relations are

$$\begin{aligned} \epsilon_r &= \frac{\partial u}{\partial r} \qquad \epsilon_z = \frac{\partial w}{\partial z} \\ \epsilon_\theta &= \frac{u}{R} \qquad \gamma = \frac{\partial u}{\partial z} + \frac{\partial w}{\partial r} \end{aligned} \tag{3}$$

Substituting Eq. (1) into Eq. (3), the strains can be written as

$$\{\epsilon\} = [E]\{\alpha\} \tag{4}$$

where $\{\epsilon\} = \{\epsilon_r, \epsilon_\theta, \epsilon_z, \gamma\}$ is the strain vector. Substituting Eq. (2) into Eq. (4), the strains at any point within the element can then be determined from the node displacements as

$$\{\epsilon\} = [E][D]\{x\} = [B]\{x\} \tag{5}$$

For elastic materials, the stress-strain relation can be written symbolically as

$$\{\sigma\} = [C]\{\epsilon\} \tag{6}$$

where $\{\sigma\} = \{\sigma_r, \sigma_\theta, \sigma_z, \tau\}$ is the stress vector and C the matrix relating stress to strain. Again for the axisymmetric isotropic elastic problem, the C matrix is

$$[C] = \frac{E}{(1+\nu)(1-2\nu)} \begin{bmatrix} (1-\nu) & \nu & \nu & 0 \\ \nu & (1-\nu) & \nu & 0 \\ \nu & \nu & (1-\nu) & 0 \\ 0 & 0 & 0 & \left(\frac{1-2\nu}{2}\right) \end{bmatrix}$$

where E is Young's modulus and ν is Poisson's ratio.

For the elastic problem, the procedure to obtain the motion of each node point of the element can be outlined as follows. Let us suppose that at some time, t, the six node displacements, $\{x\}$, are specified together with any applied node point forces (if any) written as

$$\{P\} = \{P_i^u, P_i^w, P_j^u, P_j^w, P_k^u, P_k^w\} \tag{7}$$

The superscript in Eq. (7) indicates the direction of the applied forces (horizontal or vertical) and the subscript i, j, or k refers to the particular node point of the element. The equations of motion for node point i can then be written simply as

$$\begin{aligned} m_i \ddot{u}_i &= P_i^u - R_i^u \\ m_i \ddot{w}_i &= P_i^w - R_i^w \end{aligned} \tag{8}$$

where m_i is the mass of node point i, and (R_i^u, R_i^w) are the effective resisting forces developed by the distortion of the element under the specified node displacements, $\{x\}$. Similar equations are developed at nodes j and k. The procedure for assigning the effective mass of each node point has been given in Ref. 1. Basically, the mass of each node is assigned so that the total mass of the three nodes is the same as the mass of the element and the centroid of the three masses coincides with the centroid of the element.

Returning to the time integration of Eq. (8), if at time t, the reaction forces (R_i^u, R_i^w) can be determined in terms of the node displacements $\{x\}$, the accelerations of each node can be computed. Knowing the accelerations at this time, the displacements of the nodes can be determined at the following time, $t + \Delta t$, by some suitable numerical integration scheme. Knowing the new displacements, the cycle can be started again by determining the accelerations from Eq. (8) at time $t + \Delta t$ and integrating to obtain the node displacements at time $t + 2\,\Delta t$, etc.

The problem remaining, then, is to determine the resisting forces developed by the node point displacements which distort the element (clearly a displacement field causing rigid body motions of the element develops no resisting forces). Prior to outlining this procedure, it should be mentioned that the equations of motion actually integrated are not those of the individual elements, as Eq. (8), but rather the total node point equations. If one considers all the elements connected at a given node (Fig. 2), the node point equations of motion become

$$\begin{aligned} M_N \ddot{u}_N &= F_{uN}^A - \sum F_{uN}^R \\ M_N \ddot{w}_N &= F_{wN}^A - \sum F_{wN}^R \end{aligned} \tag{9}$$

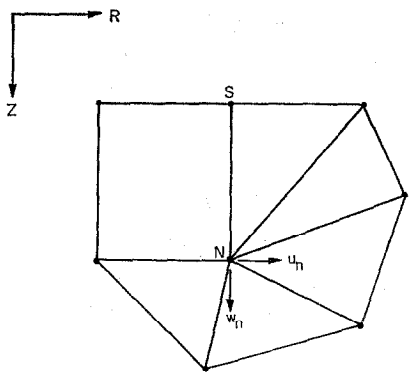

FIG. 2. Typical interior node point, N, and surrounding node points, S.

where M_N is the total node mass composed of the contributions from each adjacent element, and the node resisting forces are the sum of those obtained from each of the adjacent elements.

Elastic Resisting Forces

The resisting forces developed by the given node displacements $\{x\}$ can be obtained as follows. Consider virtual displacements $\{\delta x\}$ of the nodes. These virtual displacements cause virtual strains (Eq. 5)

$$\{\delta\epsilon\} = [B]\{\delta x\} \tag{10}$$

The associated strain energy developed in the element is then

$$\delta W_i = \int_V \{\delta\epsilon\}' \{\sigma\}\, dV \tag{11}$$

where the prime indicates the transpose, and the integral is taken over the volume of the element. The stresses $\{\sigma\}$ are related to the actual node displacements by Eq. (5) and (6) as

$$\{\sigma\} = [C][B]\{x\} \tag{12}$$

Substituting Eq. (10) and (12) into Eq. (11), the strain energy developed by the virtual displacements is

$$\delta W_i = \{\delta x\}' \left[\int_V [B]'\,[C][B]\, dV\right] \{x\} \tag{13}$$

The corresponding external work done by the equivalent nodal resisting forces $\{R\}$ during the virtual displacement is

$$\delta W_e = \{\delta x\}' \{R\} \tag{14}$$

where $\{R\} = \{R_i^u, R_i^w, R_j^u, R_j^w, R_k^u, R_k^w\}$. Equating the internal and external work, the equivalent node resisting forces corresponding to the node displacements are

$$\{R\} = \left[\int_V [B]'\,[C][B]\, dV\right] \{x\} \tag{15}$$

or

$$\{R\} = [k]\{x\} \tag{16}$$

The matrix $[k]$ is the element "stiffness" matrix. Again by comparing Eq. (16) with Eq. (9), the system equations of motion can be written symbolically as

$$M\ddot{x} + Kx = F^A \tag{17}$$

where M is the node mass, $\ddot{x}$ is the node acceleration (either u or w) and F^A are the applied node point forces. The system stiffness matrix, K, is obtained by suitably summing the adjacent element stiffness matrices.

Nonlinear Material Behavior

The effect of nonlinear material properties comes into play when computing the resisting forces developed by the given node displacements. The stress–strain relation for the nonlinear materials considered herein can be written as

$$\{\sigma\} = [C]\{\epsilon^T - \epsilon^N\} \tag{18}$$

or

$$\{\sigma\} = [C]\{\epsilon^E\} \tag{19}$$

where $\{\epsilon^T\}$ is the total strain vector, $\{\epsilon^N\}$ is the nonlinear strain component of the total strain, and $\{\epsilon^E\}$ is the elastic or recoverable portion of the strains. For velocity dependent constitutive relations, obvious modification to Eq. 18 or 19 must be made.

Again, considering virtual node displacements, Eq. (11) can be written as

$$\delta W_i = \int_V \{\delta x\}' [B]' \{\sigma\} \, dV \tag{20}$$

and the equivalent resisting node forces as

$$\{R\} = \int_V [B]' \{\sigma\} \, dV \tag{21}$$

Substituting Eq. (18) into (21), the resisting node forces can be found from

$$\{R\} = \int_V [B]' [C]\{\epsilon^T\} \, dV - \int_V [B]' [C]\{\epsilon^N\} \, dV \tag{22}$$

From Eq. (5) and Eq. (16), this becomes

$$\{R\} = [k]\{x\} - \int_V [B]' [C]\{\epsilon^N\} \, dV \tag{23}$$

The first term of Eq. (23) leads to the same system stiffness matrix of Eq. (17), applicable to the elastic problem, while the second term leads to corrective forces which account for the nonlinearities in the material properties, or deviations from the elastic case. The system equations of motion for each node can then be written as

$$M\ddot{x} + Kx = F^A + F^N \tag{24}$$

where the nonlinear corrective forces are determined from the element corrective forces written as

$$\{R^N\} = \int_V [B]' [C]\{\epsilon^N\}\, dV \tag{25}$$

Thus, for each element, the forces $\{R^N\}$ must be computed at each stage of the numerical integration process, suitably accounting for the previous stress–strain history of each element.

For the plane (strain or stress) triangular element, the strain distribution developed by the assumed displacement pattern is uniform over the element. Thus Eq. (25) can be simplified to

$$\{R^N\} = [P]\{\epsilon^N\} \tag{26}$$

where

$$[P] = \int_V [B]' [C]\, dV$$

For the axisymmetric triangular element and for all cases using rectangular elements, the strain distribution is variable over the element. Thus, the nonlinear strains should be computed at many points over the element cross-section to allow for a proper volume integration of Eq. (25). For our purposes, however, considering sufficiently small element sizes, the nonlinear stress and strain history is considered only at the centroid of each element and the nonlinear strains are taken as uniform over the element. This allows the use of Eq. (26) for all element shapes of interest, suitably simplifying the developed computer program.

In the following paragraphs, the derivation of the computational schemes used for the two elastic-plastic constitutive laws considered herein is outlined.

Mises Yield Criterion

This material law was chosen since (a) it has some applicability to real materials of interest, (b) it is completely specified analytically, and (c) some analytic stress wave propagation solutions are available for comparison purposes. The effective stress of the material is defined as (Ref. 2)

$$s^2 = \sigma_r^2 + \sigma_\theta^2 + \sigma_z^2 - \sigma_r\sigma_\theta - \sigma_\theta\sigma_z - \sigma_z\sigma_r + 3\tau^2 \tag{27}$$

where $(\sigma_r, \sigma_\theta, \sigma_z, \tau)$ define the state of stress at a point in the material. If a given state of stress lies below some allowable effective stress level at some instant of time, the material behaves elastically. If the effective stress equals the allowable, the tendency for plastic flow exists. The plastic behavior of the material is defined by some given effective stress-effective plastic strain relation, such as that shown in Fig. 3. Such a relationship for this type material can be easily obtained from the

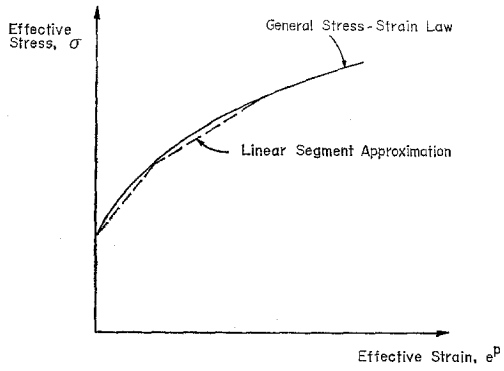

FIG. 3. Typical effective stress–strain relation for general mises material.

results of a simple tension or compression test of the material. In the developed code, any arbitrary effective stress-plastic strain curve is allowed by representing it as a series of straight line segments. If the yield curve is linear, the material is said to be linear strain hardening. If the curve is flat (constant yield stress), the material is labeled perfectly plastic.

If at a given instant of time, a stress state yields an effective stress which lies on the yield curve of Fig. 3, the tendency of the material to flow plastically is specified by the usual normality condition to be

$$\begin{Bmatrix} \dot{\epsilon}_r \\ \dot{\epsilon}_\theta \\ \dot{\epsilon}_z \\ \dot{\gamma} \end{Bmatrix}^P = \lambda \begin{bmatrix} 2 & -1 & -1 & 0 \\ -1 & 2 & -1 & 0 \\ -1 & -1 & 2 & 0 \\ 0 & 0 & 0 & 6 \end{bmatrix} \begin{Bmatrix} \sigma_r \\ \sigma_\theta \\ \sigma_z \\ \tau \end{Bmatrix} \tag{28}$$

where the superscript P indicates that the strain rate vector is associated with plastic flow and λ is some factor of proportionality. If plastic flow does occur, the amount of plastic strain is then given by

$$\{\Delta\epsilon\}^P = \Delta e^P \{\dot{\epsilon}\}^P \tag{29}$$

where Δe^P is the increment in the effective plastic strain. The total effective plastic strain is then given by

$$e^P = \sum \Delta e^P \tag{30}$$

where the sum is obtained by adding the effective strain increments developed during each time increment.

The numerical procedure then follows in a relatively straightforward manner. At some instant of time, t_i, the complete solution is known, including

node displacements	$\{x\}_i$
stresses	$\{\sigma\}_i$
effective stress	s_i
effective plastic strain	e_i^P
plastic strains	$\{\epsilon\}_i^P$
elastic strains	$\{\epsilon\}_i^E$
total strains	$\{\epsilon\}_i^T$

The plastic strain rates at this time, $\{\dot{\epsilon}\}_i^P$, can then be found from Eq. (28) (to within some constant).

At the following time, $t_{i+1} = t + \Delta t$, the node displacements, $\{x\}_{i+1}$, are obtained by suitably integrating the node equations of motion. From Eq. (5), the corresponding total strains in the element, $\{\epsilon\}_{i+1}^T$, can be computed. If it is now assumed that the changes in total strain from t_i to t_{i+1} occurred elastically, an artificial stress state can then be computed by

$$\{\bar{\sigma}\}_{i+1} = [C][\{\epsilon\}_{i+1}^T - \{\epsilon\}_i^P] \tag{31}$$

and the associated effective stress, s_{i+1}, can be found from Eq. (27).

If this effective stress lies on or below the yield curve (equal to or less than the previous effective stress), the artificial stress state is a correct one, and no new plastic flow has occurred during the time increment. If this effective stress lies above the yield curve, it is incorrect and plastic flow must have occurred during this increment. The amount of this plastic flow must now be determined.

If the increment in total strains is assumed to occur fully plastically, another artificial stress state is obtained equal to the previous stress state (since the elastic strains are the same), that is

[redacted]

ment lies somewhere between these two states, as shown in Fig. 4. To obtain the

final solution, a simple trial and error procedure can be used. For the case where the yield curve of Fig. 4 is locally linear, the value of the effective plastic strain increment can be obtained analytically in terms of the local slope of the yield curve.

It should be noted that this development is based on the assumption that the strain rate vector at the beginning of thetime increment can be used over the entire increment. If the total strain increment is relatively small, this assumption is fairly

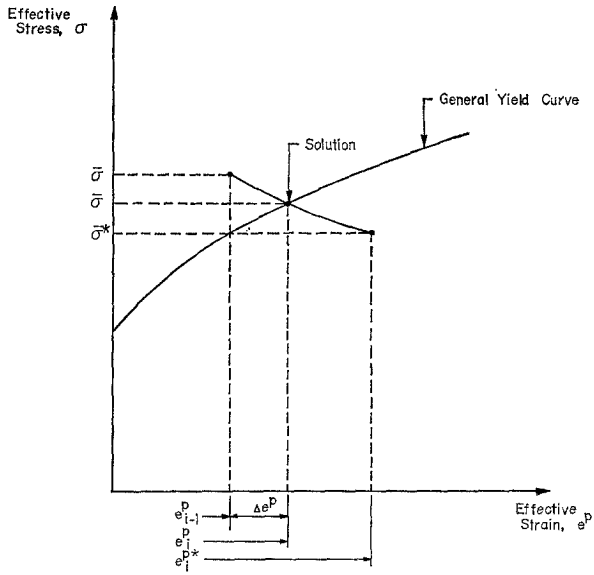

FIG. 4. General solution technique for strain increments.

good. If the increment is large, however, the assumption may lead to obvious errors. In this case, the total increment can be divided into smaller segments and a new strain rate vector computed at the end of each segment.

COULOMB–MOHR PLASTIC FLOW THEORY

For the Coulomb–Mohr plastic yield criterion, the yield surface is defined by (3)

$$f = \alpha I_1 + \sqrt{I_2'} = k \tag{33}$$

where

$$I_1 = \sigma_r + \sigma_\theta + \sigma_z$$
$$I_2' = \tfrac{1}{6}\{(\sigma_r - \sigma_\theta)^2 + (\sigma_\theta - \sigma_z)^2 + (\sigma_z - \sigma_r)^2\} + \tau^2$$

and α and k are material properties related to the usual soil properties, the angle of internal friction and cohesion. When the stress state lies within the yield surface ($f < k$), the material is assumed to behave elastically, whereas if the stress state lies on the yield curve ($f = k$), the potential for plastic flow exists. Considering principal stress space, the yield surface is a cone whose axis makes equal angles with the (σ_1, σ_2, σ_3) axes (Fig. 5). The Mises yield surface, by comparison, is a circular cylinder which has the same axis as the conical surface of the Coulomb–Mohr theory. Thus, Coulomb–Mohr materials have plastic flow properties dependent upon the mean normal stress whereas the Mises materials, as previously defined, do not.

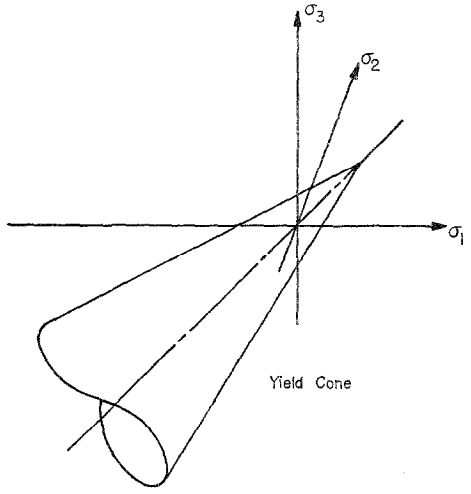

FIG. 5. Coulomb–Mohr yield surface.

If the friction angle (ϕ) and cohesion (c) of soils are determined from a triaxial compression test, the parameters (α, k) of the yield criterion may be found by

$$\alpha = \frac{2c}{\sqrt{3}} \frac{\sin \phi}{(3 - \sin \phi)}$$
$$k = \frac{6c}{\sqrt{3}} \frac{\cos \phi}{(3 - \sin \phi)} \tag{34}$$

As for the Mises material, the plastic strain rates are obtained from the normality condition, or

$$\begin{Bmatrix} \dot{\epsilon}_r \\ \dot{\epsilon}_\theta \\ \dot{\epsilon}_z \\ \dot{\gamma} \end{Bmatrix}^P = \alpha\lambda \begin{Bmatrix} 1 \\ 1 \\ 1 \\ 0 \end{Bmatrix} + \frac{\lambda}{6\sqrt{I_2'}} \begin{bmatrix} 2 & -1 & -1 & 0 \\ -1 & 2 & -1 & 0 \\ -1 & -1 & 2 & 0 \\ 0 & 0 & 0 & 6 \end{bmatrix} \begin{Bmatrix} \sigma_r \\ \sigma_\theta \\ \sigma_z \\ \tau \end{Bmatrix} \tag{35}$$

where λ is again a factor of proportionality. The dilatation rate is then

$$\dot{\epsilon}_r + \dot{\epsilon}_\theta + \dot{\epsilon}_z = 3\alpha\lambda \tag{36}$$

Thus plastic flow of such materials is associated with a volume expansion.

For the special case where the stress state is at the apex of the yield cone, Eq. (35) no longer applies since $I_2' = 0$. For this case the strain rate vector is undefined. However, it must lie within the outer normals to the conical surface at the apex.

The solution procedure is similar to that described for the Mises material. At some time, t_i, the complete solution is know, while by the integration process, the new total strains at $t_i + \Delta t$ are known. Again, a fictitious stress state can be computed by assuming that the strain increments occur elastically. From Eq. 33, the yield function, f, can be computed for this fictitious state. If $f \leqslant k$, the strain increment actually did take place elastically, while if $f > k$, the fictitious stresses are inadmissible and plastic flow did occur. Again taking the strain rate vector at the beginning of the increment, the correct solution can be obtained to yield the actual stresses and plastic strain increments that develop. This process can be slightly modified by dividing the total strain increment into a series of segments and computing the new strain rate vector at the beginning of each segment.

Other Constitutive Relations

The previous descriptions are based upon constitutive relations where the nonlinear strain components of Eq. (18) are really the nonrecoverable strain components. However the same procedure can be used to treat other materials wherein part of the nonlinear strain components can also be recovered upon "unloading". This has been done, for example, in treating materials described by the material law (g) of the catalogue mentioned previously. This material description is one that was obtained primarily by fitting experimental data that was available.

For these cases, the nonlinear strain, $\{\epsilon^N\}$, used in the equations of motion are fictitious strains used to obtain the proper corrective forces, $\{F^N\}$, in Eq. (24). For all nonlinear laws, the procedure is essentially to use the known previous stress history of the material together with the predicted current displacement and velocity fields to predict the current stress states. For these cases, then, a fictitious nonlinear strain can be obtained from Eq. (18) as

$$\{\epsilon^N\} = \{\epsilon^T\} - [C]^{-1}\{\sigma\} \tag{37}$$

Thus any nonlinear material law can be treated within the same procedure previously described.

SOME COMPARISON RESULTS

In the following paragraphs, we present some of the results obtained via the SLAM Code for particular problems and where available, comparisons with analytic solutions are made. The first set considered were the simple one-dimensional problems (stress waves in rods or about cylindrical or spherical cavities), and these were used primarily to assist in the "debugging" process.

It should be noted that the use of the two-dimensional SLAM Code for these simple problems is extremely inefficient since the computer code treats all problems as two-dimensional. By placing suitable restrictions on node point motions, the one-dimensional behavior can be suitable simulated, but with a corresponding waste of computer time. This point can be more clearly seen by considering the constrained rod problem.

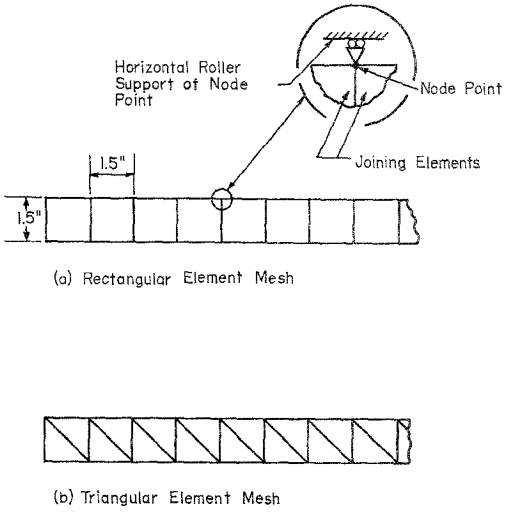

FIG. 6. Mesh types used for plane and cylindrical wave problems.

To investigate this problem, a finite element mesh was constructed of uniform rectangles, as shown in Fig. 6. To simulate the constrained motion, each node point of the mesh was restricted to move in the horizontal direction only by considering each node to be on a horizontal roller support. Each node has then only one degree of freedom and a single equation of motion for each node is numerically integrated with time. Therefore, at each station (distance from the end of the rod), two equations of motion are integrated, one for the top node and one for the bottom. If one were to write a computer program for this one-dimensional problem, only a

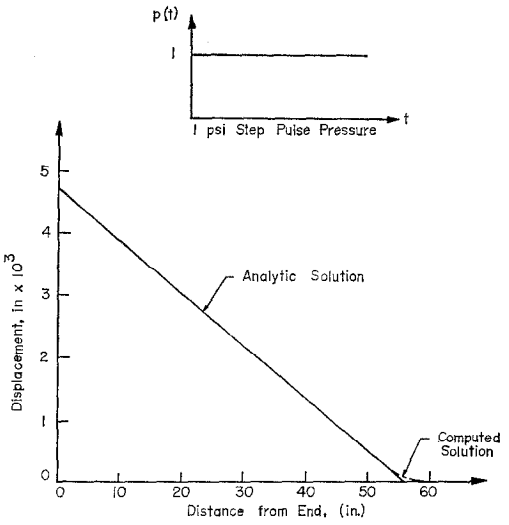

FIG. 7. Displacement variation at $t = 6.28$ msec, one-dimensional plane strain problem, rectangular elements, elastic material.

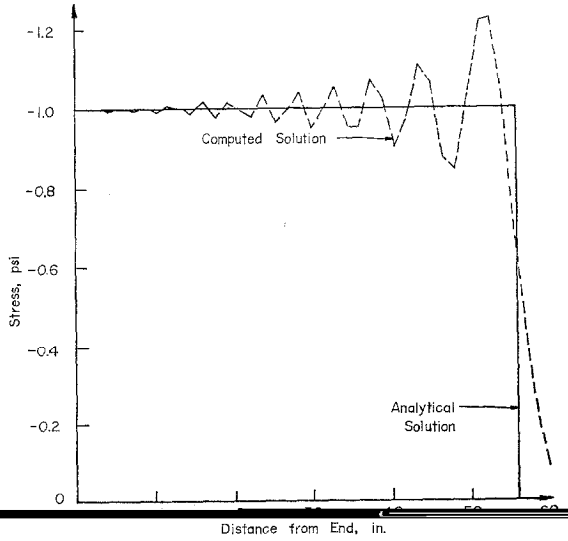

FIG. 8. Horizontal stress variation at $t = 6.28$ msec, one-dimensional plane strain problem, rectangular elements, elastic material.

single equation of motion would be considered at each station. Nonetheless, the use of this simple problem serves as a check on the two-dimensional SLAM Code.

A computer solution was obtained using the mesh of Fig. 6 and assuming the material to be elastic ($E = 10^4$ psi, $v = 0.25$, w (unit weight) = 100 pcf). A step pulse pressure of 1 psi magnitude was applied to the end of the rod. The displacement variation along the rod at a specific time after load application is shown in Fig. 7, from which it may be noted that the only differences between the computed and analytic solutions occur at the front (the sharp step front is "smeared" out across several mesh widths). This can be better seen in Fig. 8, which is a plot of the horizontal stress variation along the rod at the same time. The sharp stress front, which cannot be handled by the finite approximation techniques (including any finite difference techniques), is smeared which leads to the usual oscillations about the true solution behind the front, which then gradually decay. This smearing effect on stress fronts can, of course, be minimized by the inclusion of "artificial viscosity" terms in the equations of motion, as has often been done in the various finite difference codes. This has not been used for the results presented herein as shock formation was not of interest for these problems.

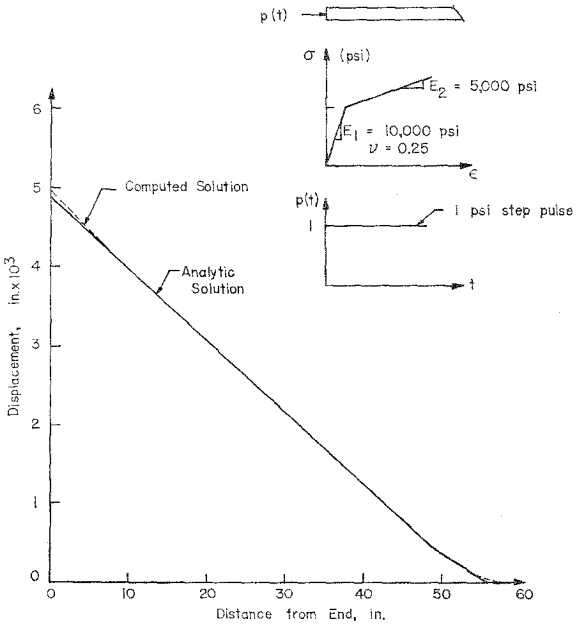

FIG. 9. Displacement variation at $t = 6.28$ msec, one-dimensional plane strain problem, rectangular elements, mises material.

As mentioned, the mesh used for this problem was the rectangular mesh of Fig.6. The equations of motion developed are then entirely analogous to those that would accrue by the finite difference methods, since the nodes are spaced uniformly. The same problem was run using the triangular element mesh of Fig. 6b, with no noticeable difference in the computed results. Again, this was done to check out the developed code.

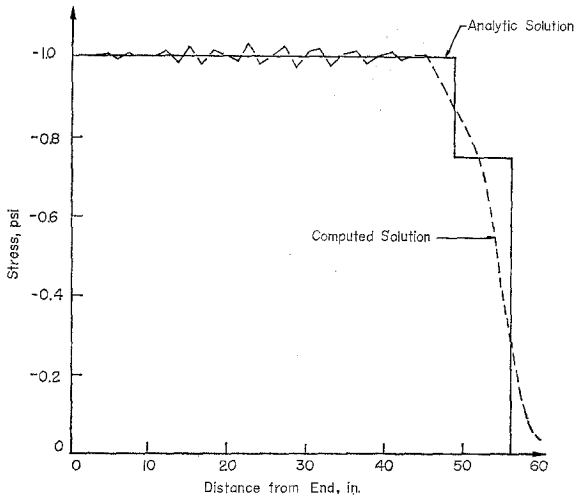

FIG. 10. Horizontal stress variation at $t = 6.28$ msec, one-dimensional plane strain problem, rectangular elements, mises material.

The next problem considered was the same as the previous one with the exception that the material was assumed to behave as an elastic-Mises plastic material with a yield stress of $\frac{1}{2}$ psi and a secondary modulus of 5,000 psi; that is, the slope in simple compression beyond the elastic limit is 5000 psi (strain-hardening). Again, the displacement variation along the rod at a specific time is shown in Fig. 9. The displacement computations are as before in good agreement with the analytic solution. The corresponding horizontal stress variation in the rod is shown in Fig. 10. By comparing these results with those of Fig. 8 for the elastic problem, it may be noted that the magnitude of the oscillations in the computed stresses is much lower than in the elastic problem due to the plastic dissipation effects. The sharp fronts (two in this case) are again smeared out across several mesh widths.

Using the same meshes of Fig. 6a and 6b, the corresponding plane stress or unconstrained problem was investigated (removal of node restrictions) as well as the cylindrical wave problem. The results of several runs for the cylindrical problem with differing strain hardening moduli is shown in Fig. 11, clearly indicating the

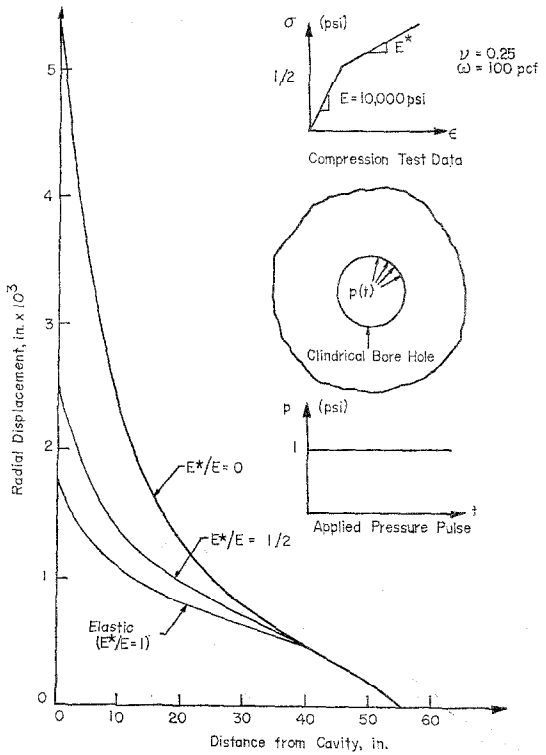

FIG. 11. Displacement variation at $t = 6.28$ msec, cylindrical wave problem, step pulse pressure, rectangular mesh, mises material.

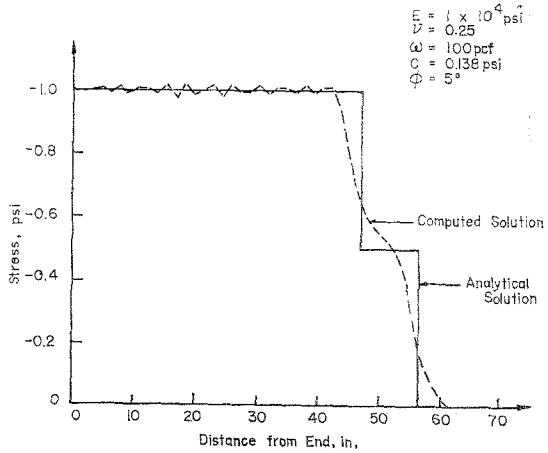

FIG. 12. Stress variation at $t = 6.28$ msec, one-dimensional plane strain problem, rectangular elements, Coulomb–Mohr material.

influence of plastic flow on the response. A typical result for a Coulomb–Mohr material is shown in Fig. 12, the geometry again being the plane strain rod problem. The material in this case exhibits both internal friction and cohesion. Other spherical wave problems including effects of load and unload were run and compared with other numerically generated data with similar results obtained. These have not been included here for brevity.

Ground Shock Problem

Among the various two dimensional problems for which numerical data was generated included a particular layered half-space subjected to the pressure loadings simulating the effects of a nuclear detonation. The configuration and applied loadings of the half space are shown in Fig. 13. The loadings used to

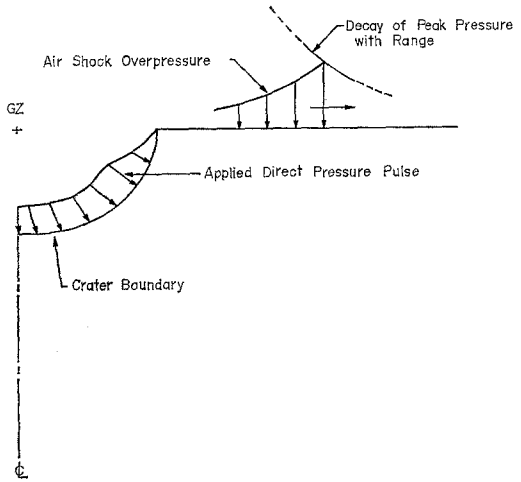

Fig. 13. Applied loadings to simulate nuclear detonation.

simulate the blast effects include a surface overpressure radiating from ground zero together with a direct pressure pulse. This direct pulse is used to simulate the effects of the direct ground shock emanating from the crater. The results of "close-in" codes, specifically designed to treat this ultra high pressure region, have been used to generate the form and phasing of this pulse.

The half-space is composed of three rock layers, each with differing properties. The surface layer, extending to the 50 ft. depth, is a shale material with properties represented by an elastic-Mises plastic material. The second layer extends to 200

feet and is a Limestone, represented as an elastic-Coulomb–Mohr material. The third layer is the base layer and is an elastic granite material. The specific properties of each rock is presented in Table 1.

TABLE 1

ROCK PROPERTIES

Layer	Depth (ft)	Elastic Properties	Plastic Properties
Shale	0–50	$E = 1.5 \times 10^5$ psi $\nu = 0.47$ $w = 137$ pcf	Mises plastic $\sigma y = 170$ psi $H = 0$ psi
Limestone	50–200	$E = 6.6 \times 10^5$ psi $\nu = 0.3$ $w = 143$ pcf	Coulomb–Mohr plastic $c = 4200$ psi $\phi = 21.4$ degrees
Granite	200–∞	$E = 9.6 \times 10^6$ psi $\nu = 0.25$ $w = 167$ pcf	None

A portion of the mesh that was used for this problem is shown in Fig. 14. Data was desired at some specific ground ranges and depths only. In this region, the mesh was made relatively fine. Away from this zone, the mesh was gradually coarsened

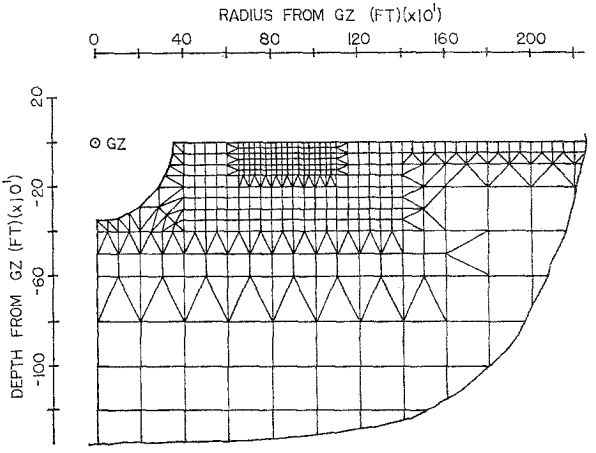

FIG. 14. Section of element mesh used in three-layer problem.

to minimize the total number of nodes (or degrees of freedom) required. The boundaries of the mesh were placed sufficiently far so that any reflection effects of the boundaries would not be felt in the zone of interest within the desired time duration. The mesh used consisted of about 700 nodes or 1400 degrees of freedom.

The vertical displacement history computed at the surface at a specific ground range (distance from ground zero) is shown in Fig. 15. Positive displacements in this figure are measured downward. The initial air induced displacement reaches a peak value of approximately 5 inches after which the direct pressure pulse traverses

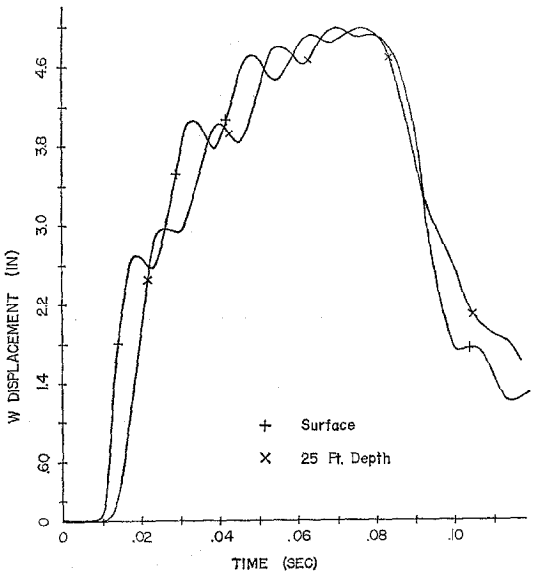

FIG. 15. Vertical displacement history, 700 ft. ground range.

the site causing the upward motion. Similar computations for a half space composed entirely of the elastic granite base layer material showed a peak vertical displacement of 1.5 inches. Thus the plastic flow effects in the surface layers significantly increase the developed displacements.

At the deeper depths in the elastic granite, the corresponding vertical displacement histories (Fig. 16) are significantly reduced and are also different in character, with the direct induced effects not as great as at the surface. The oscillations in the motions in Fig. 16 are caused by the layering of the system which induce a significant bounce effect in the gross motion.

The horizontal or radial displacement history developed at the surface is shown

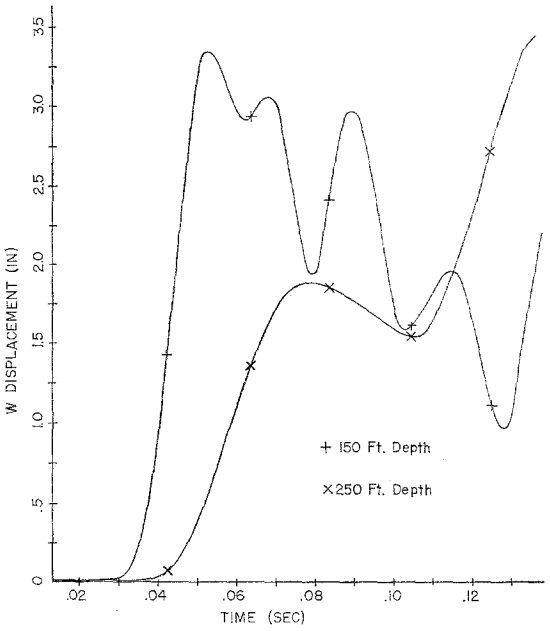

FIG. 16. Vertical displacement histories, 700 ft. ground range.

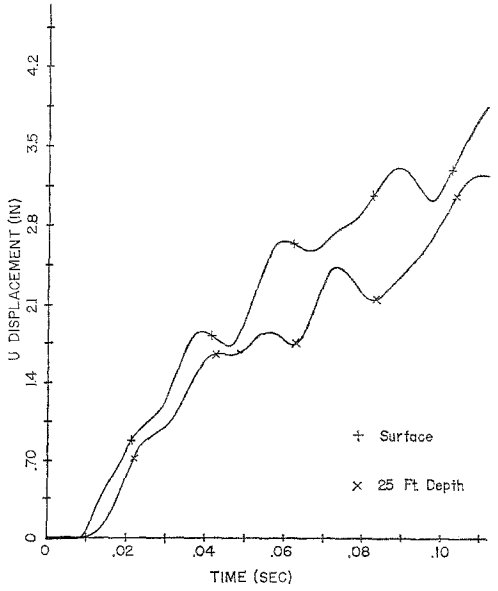

FIG. 17. Horizontal displacement histories, 700 ft. ground range.

noted, the motion is entirely outward at the surface. Again, comparing the results with those for the uniform elastic problem, plastic flow effects completely change the radial response. For the elastic problem, the shear wave effects cause the air-induced surface motion to be initially inward (toward ground zero). This is then reversed with the passage of the direct ground shock. As can be seen from Fig. 17, the weakness of the material in shear prevents this initial inward motion from occurring.

Conclusions

This paper has presented a summary of the development of a large computer program designed to treat the general two-dimensional stress wave propagation problem. The code is based upon the finite element formulation and considers general nonlinear plastic flow effects in the material.

The results presented for the one-dimensional wave problems were used primarily to assist in the debugging process, since these are the only problems for which analytic solutions are known. A second set of problems were investigated and these were the two dimensional steady problems of a step pressure pulse moving uniformly over the surface of a half-space. The results of these have not been presented herein for lack of space, but they were conducted to study the effect of mesh spacing on the computed responses. These indicate that expanding the mesh away from zones of interest does not significantly alter the computed response within the zones of interest. This then allows the user the capability to expand the mesh away from zones of interest to decrease the number of nodes to be considered in a problem with a corresponding decrease in computer running time.

Acknowledgment

This work was conducted for the Air Force Space and Missile Systems Organization on Contract Number F04694-67C-0808, with IIT Research Institute, Chicago, Illinois.

References

1. C. J. Costantino, Finite element approach to stress wave problems. *J. Eng. Mech. Division* **ASCE**, April (1967).
2. R. Hill, "Mathematical Theory of Plasticity." Oxford University Press, Oxford, 1950.
3. D. C. Drucker and W. Prager, Soil mechanics and plastic analysis or limit design. *Quar. Applied Math.* **10**, 157–165 (1952).